DOI: 10.1002/chem.201302912

Unzipping Nucleoside Channels by Means of Alcohol Disassembly

Julie P. Vanegas,[a] Lucas E. Peisino,[a, d] Salvador Pocoví-Martínez,[a] Ramón J. Zaragozá,*[b] Elena Zaballos-García,[c] and Julia Pérez-Prieto*[a]

Abstract: Gold nanoparticles capped with simple adenosine derivatives can form colloidal aggregates in nonpolar solvents. Theoretical calculations indicate the formation of organic channels by the supramolecular assembly of the nanoparticles by means of hydrogen bonds between the adenine moieties. The aggregates were only negligibly sensitive to *n*PrOH, *i*PrOH, and *t*BuOH, whereas some showed a similar response to MeOH and EtOH, and others showed high selectivity toward MeOH. DNA nucleoside derivatives (1-(2-deoxy-β-D-ribofuranosyl)-5-methyluracil and 2′,3′-*O*-isopropylideneadenosine) as well as thymine and other aromatic compounds such as pyrene derivatives (pyrene, 1-chloropyrene, 1-hydroxypyrene, (1-pyrenyl)methanol, and 2-hydroxynapthalene) did not induce disassembly of the nanoparticle aggregates. Data suggest that the nucleoside channels allow access to alcohols according to their size, and an efficient interaction between the alcohol and the adenine units destabilizes the hydrogen bonds, which eventually leads to nanoparticle disassembly.

Keywords: alcohols · gold · hydrogen bonds · nanoparticles · nucleosides

Introduction

Spherical nanoparticles (NPs) can be used as a platform for the incorporation of a considerable number of specific functionalities on their periphery owing to their high surface-to-volume ratio, thus making it possible to have a high local concentration of a functional group in an otherwise very diluted solution. In particular, gold nanoparticles (AuNPs) are of great interest owing to their unique electronic and chemical properties, which are size-dependent.[1–3] Nanometer-sized gold particles exhibit intense colors owing to light absorption in the visible region; as a consequence, nanoparticles at nanomolar concentrations can be clearly observed by the naked eye. In addition, they exhibit strong distance-dependent optical properties.

The assembly of specifically derivatized AuNPs leads to a redshift and widening in the extinction band, and thus blue colloidal solutions are obtained. Most of these systems use large biomolecules, such as oligonucleotides, DNA, and proteins at the NP periphery.[4–10] Interactions that occur at this periphery are responsible for the formation of stable aggregates, and some small molecules might help in the aggregation process. In the latter case, the strategy results in a practical tool for the development of colorimetric sensing of the molecule. Alternatively, aggregated NPs can be disassembled by metal ions or other analytes, and the color of the colloid gradually changes from blue to red. Therefore, aggregated NPs can also be used in colorimetric sensing.[7,10] Sensors based on metal NPs capped with small ligands are less common and they use analyte-induced NP aggregation as their sensing strategy.[11–15]

We report here that experimental results together with theoretical calculations suggest that hydrogen bonding between adenine (AD) units around the periphery of AuNPs can lead to AuNP assembly and, consequently, the formation of organic channels between the aggregated AuNPs. These aggregates can exhibit size-selective inclusion of light alcohols, which cause unzipping of the nucleosides channels and, eventually, lead to AuNP disassembly.

Results and Discussion

Assembly of AuNPs capped with adenine moieties in low-polar solvents: First, we prepared oleylamine-stabilized AuNPs (Au@OA)[16] with an average core diameter of

[a] J. P. Vanegas, L. E. Peisino, Dr. S. Pocoví-Martínez, Dr. J. Pérez-Prieto
Instituto de Ciencia Molecular (ICMol)
Universidad de Valencia, C/Catedrático José Beltrán 2
46980 Paterna, Valencia (Spain)
Fax: (+34) 963543273
E-mail: julia.perez@uv.es

[b] Dr. R. J. Zaragozá
Departamento Química Orgánica, Facultad de Quimica
Universidad de Valencia, Dr. Moliner, 50
46100 Burjassot (Spain)
E-mail: ramon.j.zaragoza@uv.es

[c] Dr. E. Zaballos-García
Departamento Química Orgánica, Facultad de Farmacia
Universidad de Valencia
C/Vicent Andrés Estellés s/n, 46100 Burjassot (Spain)

[d] L. E. Peisino
Current address: INFIQC, Departamento Química Orgánica
Universidad Nacional de Córdoba, Ciudad Universitaria
5000 Córdoba (Argentina)

Supporting information for this article is available on the WWW under http://dx.doi.org/10.1002/chem.201302912.

(9.51 ± 2.97) nm. These NPs gave rise to burgundy solutions in chloroform, and their UV-visible absorption spectrum exhibited the typical plasmon band at $\lambda_{max} = 525$ nm (see Figure S1 in the Supporting Information). Then they were used as precursors of different types of AuNPs (Au@H_2N-AD_1, Au@S-AD_1, and Au@S-AD_2; see Figure 1A) capped with

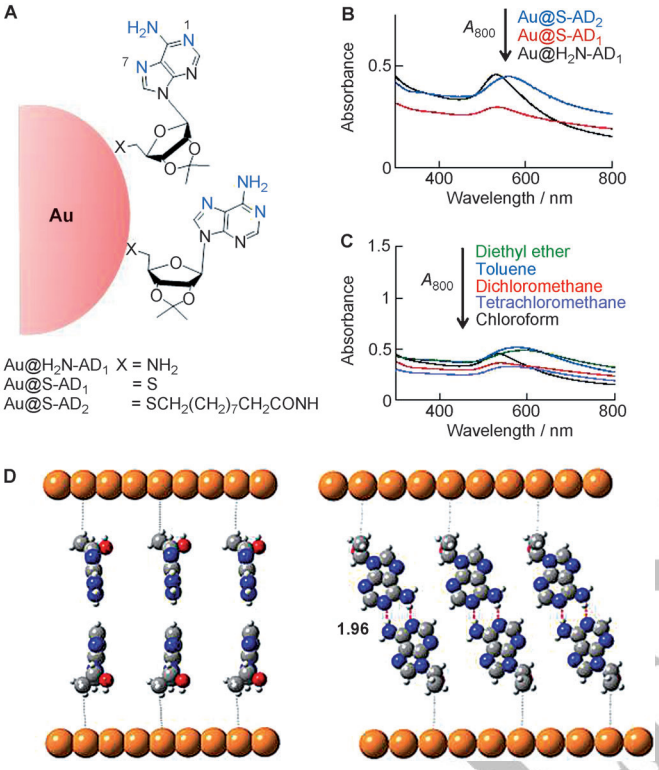

Figure 1. A) AuNPs capped with AD derivatives, B) comparison between the UV/Vis absorption spectra of the NPs in chloroform, and C) UV/Vis absorption spectra of Au@H_2N-AD1 in different solvents. D) Theoretical assembly by hydrogen bonds between two NPs. The distance between the AuNP surface and the adenosine residues is not drawn to scale. The displayed hydrogen-bond length is in Å.

AD derivatives with different types of anchoring groups (NH_2, S), as well as different chain lengths that connected the anchoring group to the sugar unit (CH_2, $(CH_2)_{10}CONH$); see details in the Experimental Section and Figures S2–S5 in the Supporting Information. The exchange of oleylamine ligands by H_2N-AD_1[17] was carried out by stirring the NPs dissolved in chloroform in the presence of the amine.[18] The redshift in the plasmon peak accompanied by a considerable broadening of the spectrum evidenced the decrease in the interparticle distance and suggested hydrogen-bond interactions between the adenine moieties located around the periphery of different NPs (Figure 1B).

The aggregates, which are typically blue, proved stable in chloroform. The assembly of Au@H_2N-AD_1 was also analyzed in other low-polar solvents, such as dichloromethane, tetrachloromethane, toluene, and diethyl ether. UV-visible spectra evidenced that the aggregation degree was dependent on the nature of the solvent (Figure 1C).

It has previously been reported that 9-substituted AD derivatives self-associate in chloroform through the amino group and the hydrogen-bond-accepting nitrogen atoms of the aromatic rings.[19] Therefore, the assembly of the NP in low-polarity solvents confirms that the AD moieties were around the NP periphery. Similarly, HS-AD_1 and HS-AD_2 led to aggregates. Figure 1B compares the UV-visible absorption spectra of Au@H_2N-AD_1, Au@S-AD_1, and Au@S-AD_2 aggregates in chloroform.

The effect of the ligand features on the aggregation of the AD-capped NPs was estimated approximately by using a flocculation parameter, which is defined as the ratio between the integrated absorbance of the aggregate between 600 and 800 nm and that between 500 and 600 nm. This value increases with the degree of NP assembly, which is in agreement with the presence of transversal and longitudinal surface plasmons that appear upon aggregation.[20] In chloroform, the values were 1.8, 1.7, and 1.0 for Au@S-AD_2, Au@S-AD_1, and Au@H_2N-AD_1, respectively (i.e., a better anchoring group apparently facilitated the formation of NP aggregates).

Theoretical calculations were performed to gain insight into the structure of the aggregates. The large size (9.5 nm diameter) of the nanoparticles produces a small curvature of the Au surface layer; therefore, we assumed that their surface was nearly flat and used the model of Au(111),[21] in which the Au atoms are distributed in the form of hexagonal cells with the maximum capping. The distance between the Au atoms is 2.884 Å (see Figure S6A in the Supporting Information). Previous studies indicate that linear thiols are attached to the six gold atoms at the vertices of a hexagonal arrangement on the Au surface (see blue hexagon in Figure S6A in the Supporting Information). However, the large size of S-AD_1 prevented this hexagonal arrangement and made other hexagonal geometries plausible (see hexagon in black and red in Figure S6A in the Supporting Information). Therefore, S-AD_1 was minimized (see **1** in Figure S6C in the Supporting Information) and roughly coupled to the gold surface (see Figure S6D in the Supporting Information and calculation details in the Experimental Section). The hexagonal arrangement that comprises eighteen Au atoms (hexagon marked in red in Figure S6A in the Supporting Information) permits the maximum packing of this ligand while avoiding the collapse of the van der Waals spheres between neighboring molecules (see Figure 2A).

The size of the cluster in Figure 2A made the calculation of the geometry of the organic ligands on the AuNP surface difficult at a high level of theory (B3LYP/6-31G**). Therefore, to analyze it more accurately, we simplified the model by taking into account that 1) the sugar fragment and the Au core would not be involved in the interactions around the nanoparticle periphery, and 2) the AD moieties would be responsible for the interparticle interaction and would exhibit more mobility than the other ligand moieties. Consequently, the simplified model comprised the AD moiety plus the atoms directly attached to it (i.e., C1′, C2′, and O−C1′; Figure S7 in the Supporting Information). Then we fixed the

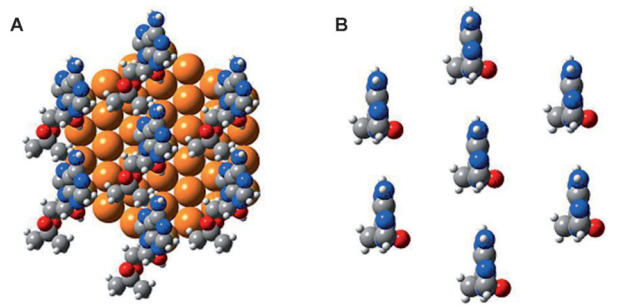

Figure 2. Three-dimensional view (van der Waals spheres) of A) the S-AD_1 moieties assembled on the Au(111) surface and B) the minimized cluster **CL**.

positions of C1′, C2′, and O−C1′ and that of their corresponding hydrogen atoms, as well as the distances between the N-9 adenine fragments. This made free rotation of the AD units possible and prevented the organic moieties from coming or separating (i.e., it simulated the anchoring of the organic units to the Au surface as well as the lateral compression exerted by the other organic moiety units, which are not depicted in the cluster). Remarkably, this brought about an almost perfect alignment of the AD units (cluster **CL** in Figure 2B); a weak hydrogen bond, specifically N3···HN−C6, between the AD units might play a role in such alignment (see Figure S8 in the Supporting Information).

The next step was to establish the cause of the NP aggregation. At this point, it was quite clear that the main reason for this assembly was the formation of hydrogen bonding between AD moieties of different nanoparticles. Such interaction would be strongly stabilized through an N1···HN−C6 hydrogen bond between the ADs (see Figure 1D). Interestingly, the alignment of the AD units of each nanoparticle induced an antiparallel arrangement between the nanoparticles and created a series of channels between the bonded AD units. We presumed that this could permit the movement of molecules of the right size within the capping of the aggregated nanoparticles. In addition, it seemed reasonable to think that disassembly of the NP aggregates could be induced through destabilization of the interparticle hydrogen bonds by increasing the alcohol concentration.

Disassembly of AuNPs capped with adenine moieties: Remarkably, the addition of increasing amounts of MeOH (aliquots of 10 μL) to the AD-capped NPs in $CHCl_3$ (1 mL) caused different states of disassembly of the NPs, as evidenced by the blueshift of the absorption up to approximately 520 nm with a concomitant narrowing of the spectrum (see Figure 3). Interestingly, the color changes occurred rapidly and, therefore, each UV-visible spectrum was registered at approximately 1 min after the addition of each MeOH aliquot. This process can be attributed to specific interactions between the AD moieties and MeOH, thereby creating repulsive forces between the NPs.

A reliable method to analyze the capacity of an analyte to induce the disassembly is by monitoring the ratio between

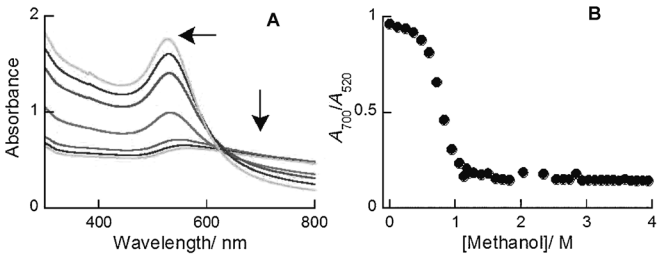

Figure 3. A) UV/Vis absorption spectra of Au@S-AD_2 aggregates in chloroform in the absence and in the presence of MeOH; the arrows indicate the absorbance trend with increasing [MeOH]. B) Plots of the A_{700}/A_{520} ratio versus [MeOH] for Au@S-AD_2 aggregates.

the absorbance at 700 nm and that of the NP plasmon peak maximum (≈520 nm); a low ratio is associated with dispersed red NPs, and a high ratio is associated with blue aggregates. Ratiometric sensors are suitable for practical applications since they are less vulnerable to fluctuations of monitoring conditions. In our study, the sensitivity of the aggregates to methanol depended on the type of NP; Figure 3B shows the A_{700}/A_{520} ratio dependence on MeOH concentration (up to 200 μL, 4 M).

In addition, EtOH was also checked as a disassembling agent. Interestingly, Au@S-AD_1 and Au@H_2N-AD_1 aggregates showed a similar response to MeOH and EtOH, but Au@S-AD_2 aggregates proved to be highly selective to MeOH. Figure 4A, C, E show the effect of adding increasing

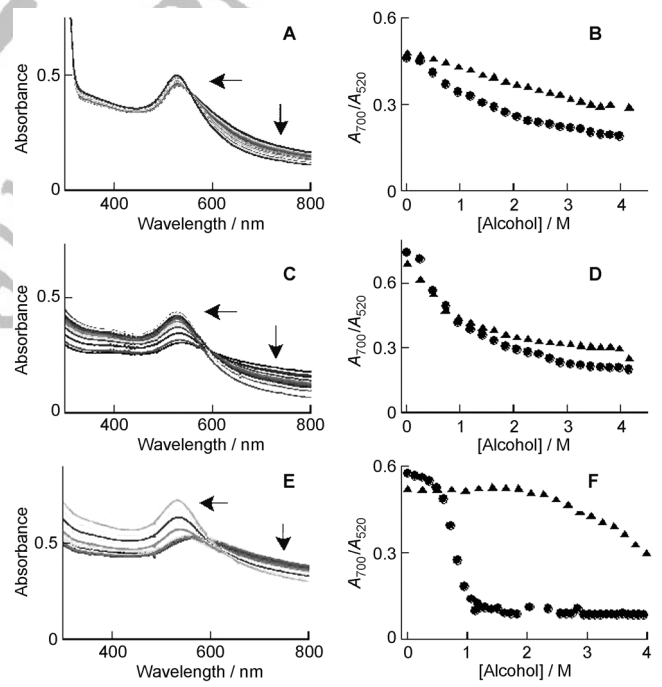

Figure 4. UV/Vis absorption spectra of A) Au@H_2N-AD_1, C) Au@S-AD_1, and E) Au@S-AD_2 aggregates in the absence and in the presence of increasing amounts of ethanol; and B, D, F) comparison between the plots of A_{700}/A_{520} versus [alcohol] for methanol (●) and ethanol (▲). The arrows in the absorption spectra indicate the absorbance trend with increasing alcohol concentrations.

ethanol concentrations to the different NPs. Figure 4B, D, F compare the A_{700}/A_{520} ratio dependence on MeOH with that on EtOH concentration. The slope of the curve and the total change of the absorbance depended on the type of NP.

The minimum detectable limit of MeOH was lower than 30 μL (in 1 mL $CHCl_3$) for Au@S-AD_2, and lower than 20 μL for the other NPs. Even though the detection limit was higher for Au@S-AD_2, owing to the presence of a lag in their response, these NPs showed the most abrupt and considerable total change in the A_{700}/A_{520} ratio; this is probably related to the length of the NP ligand. The sigmoidal dependence of the absorbance response on [MeOH] suggests a cooperative effect between the MeOH molecules and the AD units for unzipping the nucleoside channels, which finally leads to disassembly of the AuNPs (see below).

Other light alcohols, such as *n*PrOH, *i*PrOH, and *t*BuOH, were checked as disassembling agents. Interestingly, all the aggregates were negligibly sensitive to *n*PrOH, *i*PrOH, and *t*BuOH (Figure 5).

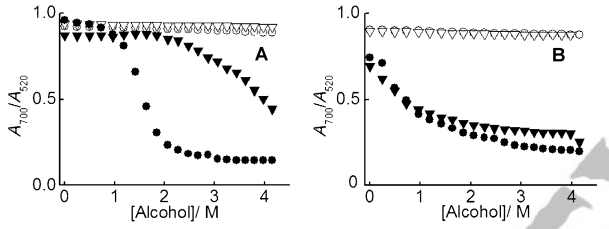

Figure 5. Comparison between the plots of A_{700}/A_{520} versus [alcohol] for A) Au@S-AD_2 and B) Au@S-AD_1 aggregates in $CHCl_3$ using different alcohols: methanol (●), ethanol (▼), isopropanol (○), and *tert*-buthanol (▽).

The image in Figure 6 shows the color changes after addition of the different alcohols to an Au@S-AD_2 aggregate and it evidences that 1) blue became fainter upon addition of increasing amounts of *i*PrOH and *t*BuOH (also *n*PrOH, not shown) due to the dilution effect; 2) the blue-to-red change was caused after addition of approximately 10 μL of EtOH, but needed approximately 20 μL in the case of MeOH; and 3) MeOH was more effective for the NP disassembly.[22] Therefore, the sensing capacity of the NP aggregates can alternatively be analyzed by measuring the absorbance at a specific wavelength. The selectivity of the AuNP aggregates to MeOH relative to the other alcohols was much greater than that shown by the majority of other MeOH sensors.[23–27]

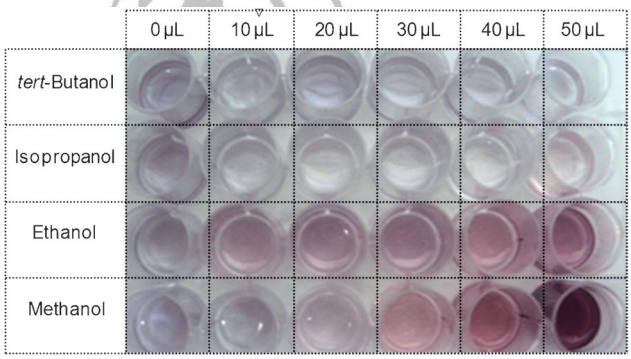

Figure 6. Images showing the effect of the addition of increasing volumes of light alcohols to solutions of Au@S-AD_2 in $CHCl_3$.

Comparison of the high-resolution transmission microscopy (HRTEM) images of the Au@S-AD_2 NPs in chloroform (1 mL) in the absence of MeOH and those in the presence of MeOH (100 μL) showed that the alcohol led to disassembly of the AD-capped AuNPs and that nanoparticle core fusion did not occur during their aggregation in chloroform (Figure 7). Moreover, the images of the nanoparticles before and after addition of 30, 40, 60, 80, and 100 μL of methanol were in accordance with the sigmoidal dependence of the A_{700}/A_{520} ratio of the colloidal solution on the MeOH concentration. Thus, a slight effect on the aggregation degree of the nanoparticles when adding methanol concentrations up to approximately 0.75 M was followed by a considerable disassembly in a short range of concentrations (from approximately 0.75 to 1 M).

The dynamic light scattering (DLS) spectra of solutions of Au@S-AD_2 NPs in chloroform (1 mL), registered before and after adding up to 60 μL of methanol (i.e., up to approximately 1.47 M of methanol), were also in accordance with the sigmoidal dependence of the aggregation degree of the nanoparticles in chloroform on the methanol concentration (Figure 8).

Moreover, control assays with different-sized molecules, which might or might not possess the capacity to be involved in hydrogen bonding with AD units, were tested for NP disassembly. We found that neither the DNA nucleoside derivative 2′,3′-*O*-isopropylideneadenosine nor even 1-(2-deoxy-β-D-ribofuranosyl)-5-methyluracil, which presents the complementary base of AD, and thymine induced disassembly of the NP aggregates. Similarly, other aromatic compounds such as pyrene, 1-chloropyrene, 1-hydroxypyrene, (1-pyrenyl)methanol, and 2-hydroxynapthalene did not cause disassembly.

We suggest the following mechanism for nanoparticle disassembly. Within the channel, the alcohol can only interact with the N7 position of the AD units, since the N1 position is blocked (see Figure 9) and the anchoring of the alcohol to N7 produces a weakening in the inter-nanoparticle hydrogen bonds and eventually induces the disassembly. In addition, as the size of the alcohol increases, the transit would be impeded and only small alcohols (MeOH, EtOH) would flow relatively easily through the channels. At this point, the alcohol would interact competitively with the N7 and N1 positions (Figure 9), thus avoiding the aggregation of the nanoparticles. In fact, we have estimated that the interaction of methanol with N1 is favored by only 0.3 kcal. In addition, as the size of the alcohol increases, the transit would be impeded, and only small alcohols (MeOH, EtOH) would flow relatively easily through the channels.

To support this hypothesis, we started by studying the hydrogen-bond interaction of the central AD unit of **CL** with a molecule of alcohol (MeOH, EtOH, *i*PrOH, and

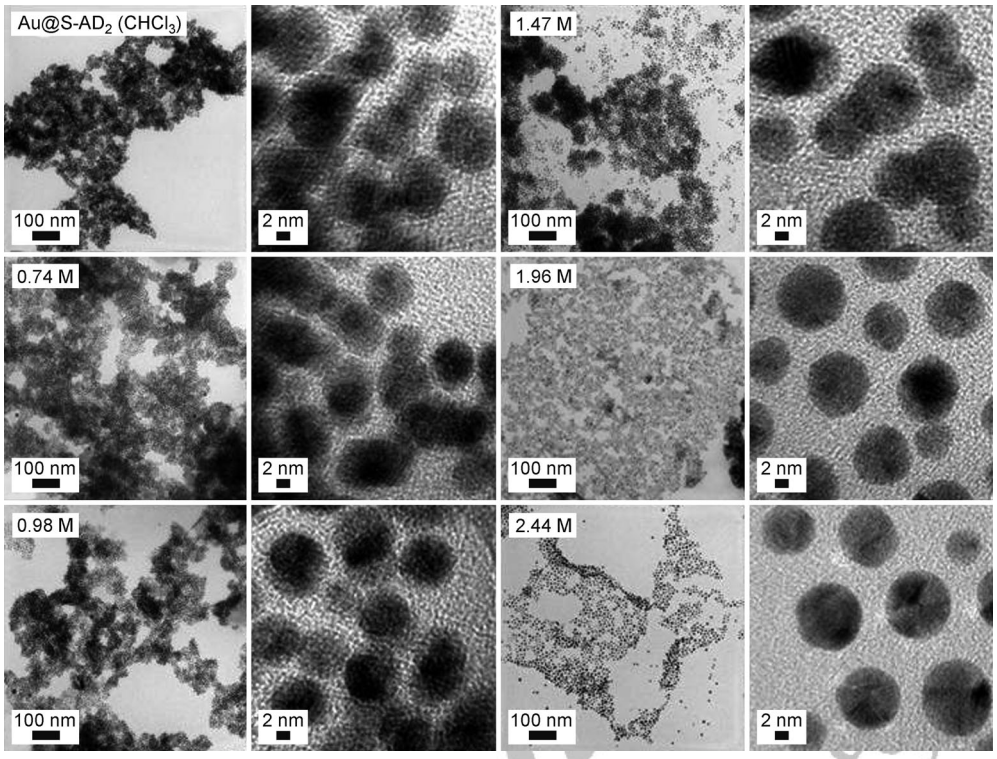

Figure 7. HRTEM images (scale bar of 100 and 2 nm) of Au@S-AD_2 in $CHCl_3$ in the presence of increasing amounts of CH_3OH (0, 30, 40, 60, 80, and 100 μL; molar concentrations at the top left-hand side of each image).

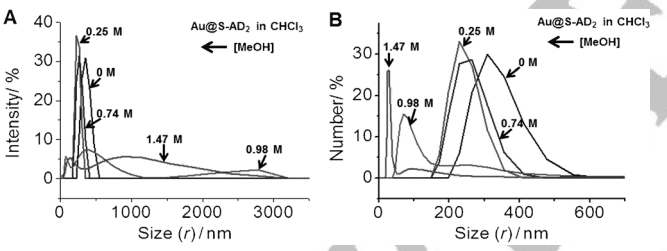

Figure 8. DLS spectra of Au@S-AD_2 in chloroform (1 mL) compared with those obtained after addition of increasing concentrations of methanol. A) Intensity versus size and B) number versus size; the methanol concentration is indicated next to each curve.

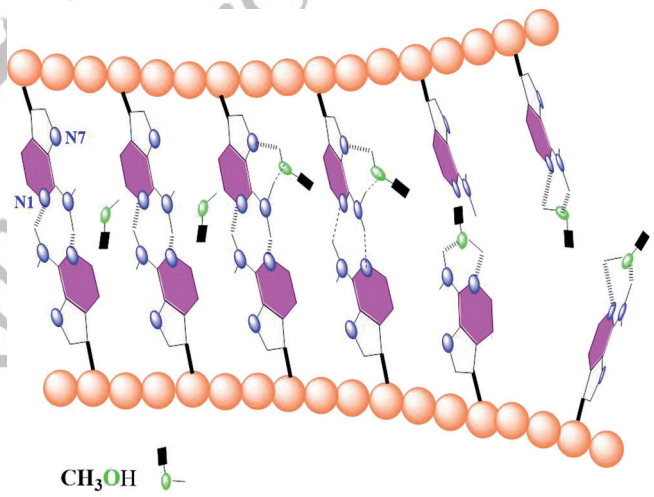

Figure 9. Pictorial representation of the cooperative action between methanol molecules and adenine units for unzipping the nucleoside channels in the NP aggregates in chloroform.

*t*BuOH)[28] through the N7 position as well as the transit of the alcohol through the organic channels (for **CL-alcohol-a** and **CL-alcohol-t**, respectively, see Figure 10A,B; Figure S9 in the Supporting Information for MeOH; and Figures S10–S12 in the Supporting Information for the other alcohols). Table 1 shows that **CL-alcohol-a** complexes were favorable from the point of view of energy (ΔE between −9.5 and −13.5 kcal mol^{-1}). However, in terms of the interaction within the channels, **CL-alcohol-t** was slightly favorable for MeOH and EtOH, a little unfavorable for *i*PrOH, and highly unfavorable for *t*BuOH (≈ −1.7 kcal mol^{-1} for MeOH and EtOH, +1.0 kcal mol^{-1} for *i*PrOH, and +36.3 kcal mol^{-1} for *t*BuOH).

In addition, since the estimations started from two separate molecular units (**CL** and alcohol) to yield a single molecular complex (**CL-alcohol**), entropic and thermal variations should also have an important contribution, together with the energy variations (ΔE), to the Gibbs free energy (ΔG). Calculation of the entropic and thermal variations requires a large amount of computation time and in some cases is not feasible owing to the large size of the molecules. Therefore, several simplifications were made in the determination of the thermal and relative thermal corrections to

Table 1. B3LYP/6-31G** total (E [au]) and relative energies (ΔE [kcal mol^{-1}]), relative thermal correction to Gibbs free energy (ΔTC-G [kcal mol^{-1}]), and relative free energies (ΔG [kcal mol^{-1}]) of the molecular complexes between cluster **CL** and MeOH, EtOH, *i*PrOH, or *t*BuOH.

	E	ΔE[a]	ΔTC-G[b]	ΔG[c]
CL	−4348.228333	–	–	–
MeOH	−115.723963	–	–	–
EtOH	−155.046200	–	–	–
*i*PrOH	−194.368581	–	–	–
*t*BuOH	−233.689169	–	–	–
CL-meoh-t	−4463.954861	−1.6	11.4	9.8
CL-meoh-a	−4463.973735	−13.5	13.2	−0.3
CL-etoh-t	−4503.277408	−1.8	11.7	9.9
CL-etoh-a	−4503.296041	−13.5	13.9	0.4
CL-isopropoh-t	−4542.595399	1.0	11.5	12.4
CL-isopropoh-a	−4542.616402	−12.2	13.5	1.3
CL-*t*-buoh-t	−4581.859646	36.3	15.9	52.2
CL-*t*-buoh-a	−4581.932564	−9.5	13.7	4.2

[a] Relative to **CL**+MeOH, **CL**+EtOH, **CL**+*i*PrOH, or **CL**+*t*BuOH. [b] From Table S1 in the Supporting Information. [c] $\Delta G = \Delta E + \Delta$TC-$G$.

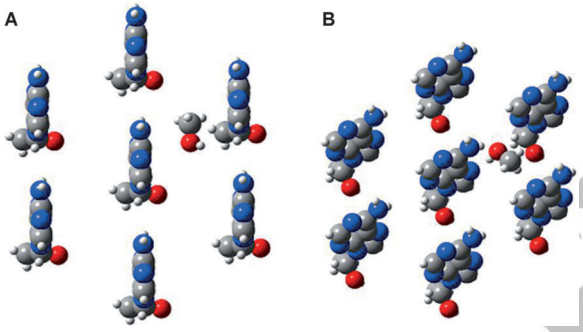

Figure 10. Three-dimensional view (van der Waals spheres) of molecular complexes between cluster **CL** and MeOH: A) **CL-meoh-t** and B) **CL-meoh-a**.

Gibbs free energy (TC-G and ΔTC-G, respectively). In this case, AD plus the atoms directly attached to it (i.e., C1′, C2′, and O−C1′) and its interaction with the corresponding alcohol were considered (see Figures S13–S16, Table S1, and further details in the Supporting Information). The data thus obtained were used in Table 1 to determine ΔG. Please note that the formation of **CL-meoh-a** is the only exergonic (−0.3 kcal mol^{-1}) process, whereas the formation of **CL-etoh-a** is slightly endergonic (+0.4 kcal mol^{-1}) and is even less favorable in the case of *i*PrOH and *t*BuOH.

These data suggest that the two smallest alcohols can flow relatively easily through the channels ($\Delta G = 9.8$ and 9.9 kcal mol^{-1}, respectively), but the transit is impeded for *i*PrOH and even prevented for *t*BuOH ($\Delta G = 12.4$ and 52.2 kcal mol^{-1}, respectively). In addition, in the case of MeOH and EtOH, there will be a considerable number of alcohol molecules interacting with the N7 atom of the AD units, since the formation of the hydrogen bond to the N7 position is favorable (**CL-meoh-a**; −0.3 kcal mol^{-1}) or just slightly unfavorable (**CL-etoh-a**; +0.4 kcal mol^{-1}). By contrast, not only the transit of the alcohol through the organic channels is more difficult in the case of *i*PrOH and *t*BuOH but also their interaction with the AD units is endergonic (+1.3 and +4.2 kcal mol^{-1} for **CL-isopropoh-a** and **CL-*t*-buoh-a**, respectively).

The anchoring of MeOH and even EtOH to the adenine N7 position should produce a weakening in the inter-nanoparticle hydrogen bonds, and, consequently, a certain number of molecules within the channel eventually trigger the NP disassembly. In fact, calculations suggest that such weakening occurs for two main reasons, one geometric and the other energetic. The geometric weakening is due to the interruption of the alignment between the AD units by introducing alcohol molecules. Thus, when the alcohol interacts with the N7 position of the AD in the center of **CL**, the AD undergoes a misalignment between 7 and 13° (see **CL-alcohol-a** in Figures S9–S12 of the Supporting Information). This effect decreases the bond strength of the hydrogen bond between the ADs (the energy variation can be quite considerable but it was not quantified). The decrease in the strength of the inter-nanoparticle bond related to energetic reasons was quantified for MeOH by using the models in Figure S20 of the Supporting Information, and we found that it is approximately 1 kcal mol^{-1} (see details in the Supporting Information).

Finally, we also carried out a preliminary study of the changes in the aggregate optical activity after addition of increasing amounts of methanol, keeping the methanol concentration well below that producing a visual change in the sample. The sign progressively reversed from negative to positive (data not shown). This indicates that in the case of chiral macromolecules, such studies would be relevant in these types of aggregates.

Conclusion

Base pairs are the building blocks of the DNA double helix and contribute to the folded structure of both DNA and RNA; hydrogen bonding is the chemical interaction that underlies the base-pairing rules. Interestingly, we have shown here that the interaction between AD units around the AuNP periphery can lead to highly stable aggregates in low-polar solvents, the stability of which is not broken in the presence of the AD complementary base, nor just by any alcohol, but by those that can penetrate the assembled structure (in particular, methanol and ethanol), thus weakening the inter-nanoparticle hydrogen bonds and eventually inducing the unzipping of the nucleoside channels. Consequently, these aggregates can be applied in the size-selective colorimetric sensing of light alcohols. Moreover, these results suggest strategies for designing porous aggregates of variable size and also of different natures, thus expanding the applicability of these systems.

Experimental Section

General: Unless otherwise specified, materials were purchased from commercial suppliers and used without further purification. Solvents were distilled prior to use. Column chromatography was carried out with silica gel Si_{60}, mesh size 0.040–0.063 mm (Merck, Darmstadt, Germany). Melting points were determined using a Sanyo–Gallencamp capillary apparatus and are uncorrected. ^1H and ^{13}C NMR spectra were recorded at 300 and 75 MHz, respectively, using a Bruker Avance DRX 300 MHz spectrometer and with deuterated chloroform ($CDCl_3$) as solvent. ^1H and ^{13}C NMR spectroscopic chemical shifts are reported in ppm and are referenced to $CDCl_3$ signals ($\delta = 7.2$ and 77.2 ppm, respectively). The coupling constants J are given in Hz. The one-bond multiplicity of carbon atoms was determined by distortionless enhancement by polarization transfer (DEPT) experiments. High-resolution mass spectral data were obtained using a VG Autospec, TRIO 1000 (Fisons) instrument. High-resolution mass spectral data were obtained using a VG Autospec, TRIO 1000 (Fisons) instrument. Electron impact (EI) at 70 eV was used in the ionization mode in mass spectra. Centrifugation was carried out using an Eppendorf Centrifuge 5804R. The absorption spectra were obtained using an Agilent 8453 spectrophotometer (UV/Vis Software ChemStation). Measurements were performed at room temperature using 4 cm^3 quartz cells. HRTEM was carried out by using a field-emission gun (FEG) TECNAI G2 F20 microscope operated at 200 kV. For preparation, AuNP samples were deposited on carbon films 24 h prior to measurement in each of the means of dispersion and dried in a vacuum. DLS measurements were carried out using a Zetasizer Nano ZS instrument at 20°C; the measurement angle was 173° backscatter, with three measurements per sample, and 13 runs per measurement. The diameter of the nanoparticles was determined by ImageJ[29] in nanometers. Statistical analysis was obtained by measuring the diameter value of 500 nanoparticles. The structure of all the compounds was determined by analytical and spectroscopic methods and by comparison with data of the compounds reported in literature.

Synthesis of the adenine-capped AuNPs (Au@H_2N-AD_1, Au@S-AD_1, Au@S-AD_2): A general procedure was used for the synthesis of Au@H_2N-AD_1, Au@S-AD_1, and Au@S-AD_2. Gold nanoparticles capped with oleylamine (Au@OA) were synthesized according to a reported procedure.[16] Then, Au@OA (0.8 mg) was added to a solution of H_2N-AD_1 (0.03 mmol) or HS-AD_1 (0.03 mmol) or HS-AD_2 (0.02 mmol) in chloroform (2 mL), and the mixture was shaken for 24 h. The NPs were recovered by centrifugation (8500 rpm) and washed several times with acetone; then they were redispersed in chloroform.

Au@H_2N-AD_1 was alternatively prepared as follows: A solution (1 mL) of H_2N-AD in water (10 mg mL^{-1}, 32.60 mM) was added to a solution (1 mL) of Au@OA in chloroform (1 mg mL^{-1}). The mixture was stirred for at least 1 h at room temperature. The organic-phase color changed from red to blue, and then all the nanoparticles went into the aqueous phase. Before stirring again, all the nanoparticles transferred back to the organic phase, the color of which changed from colorless to blue. The NPs were recovered by centrifugation (9000 rpm), washed twice with acetone, and then they were redispersed in chloroform.

General procedure for the colorimetric sensing assays: The signaling of the colorimetric sensor is based on the color change of a colloidal solution of the AuNPs; blue was associated with aggregated nanoparticles, and red was associated with nonaggregated nanoparticles. An aliquot of alcohol (10 μL each; up to a volume of 200 μL) was added to a solution of the corresponding AuNPs (0.8 mg) dispersed in the low-polar solvent (1 mL). The absorption spectrum of the sample was performed less than 1 min after each alcohol addition. In the case of the other analytes, they were previously dissolved in the same solvent as the AuNPs before their addition to the colloidal solution.

Computational methods: All calculations were carried out with the Gaussian 09 suite of programs.[30] DFT[31,32] calculations were carried out using the B3LYP[33,34] exchange-correlation functionals together with the standard 6-31G** basis set.[35]

Compound **1** (Figure S6C in the Supporting Information; SH group of HS-AD_1 substituted by an H atom) was minimized, the S atom was restored, and roughly coupled to the gold surface (Figure S6D in the Supporting Information). Thermal correction to the Gibbs free energy (TC-G) and the relative thermal correction to the Gibbs free energy (ΔTC-G) (see Figures S13–S16 and Table S1 in the Supporting Information) were calculated with the standard statistical thermodynamics at 298.15 K.

Acknowledgements

We thank MICINN (project CTQ2011-27758 and contract to S.P.M, CTQ2009-11027/BQU, CTQ2008-06777-CO2-01/BQU), GVA (ACOMP/2013/008; fellowship to J.P.V), and the Universidad de Valencia (to L.E.P) for financial support.

[1] S. Eustis, M. A. El-Sayed, *Chem. Soc. Rev.* **2006**, *35*, 209–217.
[2] L. M. Liz-Marzán, *Mater. Today* **2004**, *7*, 26–31.
[3] R. Sardar, A. M. Funston, P. Mulvaney, R. W. Murray, *Langmuir* **2009**, *25*, 13840–13851.
[4] K. Aslan, J. Zhang, J. Lakowicz, C. Geddes, *J. Fluoresc.* **2004**, *14*, 391–400.
[5] M. S. Han, A. K. R. Lytton-Jean, B. K. Oh, J. Heo, C. A. Mirkin, *Angew. Chem.* **2006**, *118*, 1839–1842; *Angew. Chem. Int. Ed.* **2006**, *45*, 1807–1810.
[6] F. Li, J. Zhang, X. Cao, L. Wang, D. Li, S. Song, B. Ye, C. Fan, *Analyst* **2009**, *134*, 1355–1360.
[7] J. Liu, Y. Lu, *J. Am. Chem. Soc.* **2004**, *126*, 12298–12305.
[8] J. Liu, Y. Lu, *Angew. Chem.* **2006**, *118*, 96–100; *Angew. Chem. Int. Ed.* **2006**, *45*, 90–94.
[9] H. Otsuka, Y. Akiyama, Y. Nagasaki, K. Kataoka, *J. Am. Chem. Soc.* **2001**, *123*, 8226–8230.
[10] W. Zhao, W. Chiuman, J. C. F. Lam, S. A. McManus, W. Chen, Y. Cui, R. Pelton, M. A. Brook, Y. Li, *J. Am. Chem. Soc.* **2008**, *130*, 3610–3618.
[11] M. Zhang, B. C. Ye, *Anal. Chem.* **2011**, *83*, 1504–1509.
[12] D. Xiang, G. Zeng, K. Zhai, L. Li, Z. He, *Analyst* **2011**, *136*, 2837–2844.
[13] S. Kado, A. Furui, Y. Akiyama, Y. Nakahara, K. Kimura, *Anal. Sci.* **2009**, *25*, 261–265.
[14] Y. Jiang, H. Zhao, N. Zhu, Y. Lin, P. Yu, L. Mao, *Angew. Chem.* **2008**, *120*, 8729–8732; *Angew. Chem. Int. Ed.* **2008**, *47*, 8601–8604.
[15] A. Gangula, J. Chelli, S. Bukka, V. Poonthiyil, R. Podila, R. Kannan, A. M. Rao, *J. Mater. Chem.* **2012**, *22*, 22866–22872.
[16] X. Lu, H. Y. Tuan, B. A. Korgel, Y. Xia, *Chem. Eur. J.* **2008**, *14*, 1584–1591.
[17] M. Kolb, C. Danzin, J. Barth, N. Claverie, *J. Med. Chem.* **1982**, *25*, 550–556.
[18] Interestingly, the addition of a solution of H_2N-AD_1 in water to solutions of Au@OA in chloroform caused the transfer of the NPs to the aqueous phase, and the NPs eventually transferred back to the chloroform phase as Au@H_2N-AD_1 agglomerates after 24 h of stirring. This strategy could be used as an alternative preparation method.
[19] L. Biemann, T. Haber, D. Maydt, K. Schaper, K. Kleinermanns, *J. Chem. Phys.* **2008**, *128*, 195103.
[20] K. S. Mayya, V. Patil, M. Sastry, *Langmuir* **1997**, *13*, 3944–3947.
[21] C. Vericat, M. E. Vela, G. Benitez, P. Carro, R. C. Salvarezza, *Chem. Soc. Rev.* **2010**, *39*, 1805–1834.
[22] All the NPs were soluble in water; however, water did not interfere in the MeOH sensing in chloroform, since the maximum amount of water soluble in the chloroform volume was approximately 1 μL, and this was insufficient for dispersing the NPs.
[23] A. A. Athawale, S. V. Bhagwat, P. P. Katre, *Sens. Actuators B* **2006**, *114*, 263–267.
[24] B. C. Sih, M. O. Wolf, D. Jarvis, J. F. Young, *J. Appl. Phys.* **2005**, *98*, 114314.

[25] V. Nechita, J. Schoonman, V. Musat, *Phys. Status Solidi A* **2012**, *209*, 153–159.
[26] G. J. Mohr, D. Citterio, U. E. Spichiger-Keller, *Sens. Actuators B* **1998**, *49*, 226–234.
[27] S. Petrova, Y. Kostov, K. Jeffris, G. Rao, *Anal. Lett.* **2007**, *40*, 715–727.
[28] In **CL-alcohol-a**, the six AD units surrounding the central one were frozen to simulate the lateral compression exerted by the other units not represented in the cluster. The central AD moiety and the alcohol molecule were allowed to move freely. In **CL-alcohol-t**, the alcohol is placed at the center of one of the channels and near the AD N7 position, and the central AD unit and the alcohol O–C were also frozen.
[29] C. A. Schneider, W. S. Rasband, K. W. Eliceiri, *Nat. Methods* **2012**, *9*, 671–675.
[30] Gaussian 09, Revision A.01, M. J. Frisch, G. W. Trucks, H. B. Schlegel, G. E. Scuseria, M. A. Robb, J. R. Cheeseman, G. Scalmani, V. Barone, B. Mennucci, G. A. Petersson, H. Nakatsuji, M. Caricato, X. Li, H. P. Hratchian, A. F. Izmaylov, J. Bloino, G. Zheng, J. L. Sonnenberg, M. Hada, M. Ehara, K. Toyota, R. Fukuda, J. Hasegawa, M. Ishida, T. Nakajima, Y. Honda, O. Kitao, H. Nakai, T. Vreven, J. A. Montgomery, Jr., J. E. Peralta, F. Ogliaro, M. Bearpark, J. J. Heyd, E. Brothers, K. N. Kudin, V. N. Staroverov, R. Kobayashi, J. Normand, K. Raghavachari, A. Rendell, J. C. Burant, S. S. Iyengar, J. Tomasi, M. Cossi, N. Rega, J. M. Millam, M. Klene, J. E. Knox, J. B. Cross, V. Bakken, C. Adamo, J. Jaramillo, R. Gomperts, R. E. Stratmann, O. Yazyev, A. J. Austin, R. Cammi, C. Pomelli, J. W. Ochterski, R. L. Martin, K. Morokuma, V. G. Zakrzewski, G. A. Voth, P. Salvador, J. J. Dannenberg, S. Dapprich, A. D. Daniels, Ö. Farkas, J. B. Foresman, J. V. Ortiz, J. Cioslowski, D. J. Fox, Gaussian, Inc., Wallingford CT, **2009**.
[31] R. G. Parr, W. Yang in *Density Functional Theory of Atoms and Molecules*, Oxford University Press, New York, **1989**.
[32] T. Ziegler, *Chem. Rev.* **1991**, *91*, 651–667.
[33] A. D. Becke, *J. Chem. Phys.* **1993**, *98*, 5648–5652.
[34] C. Lee, W. Yang, R. G. Parr, *Phys. Rev. B* **1988**, *37*, 785–789.
[35] W. J. Hehre, L. Radom, P. R. Schleyer, J. A. Pople in *Ab initio Molecular Orbital Theory*, Wiley, New York, **1986**.

Received: July 24, 2013
Published online: ■■ ■■, 0000

Feeling tipsy: Aggregates of adenosine-capped gold nanoparticles are highly stable in low-polar solvents (see figure). Their stability is not broken in the presence of other nucleosides or DNA bases, nor just by any alcohol, but by those that can penetrate the assembled structure.

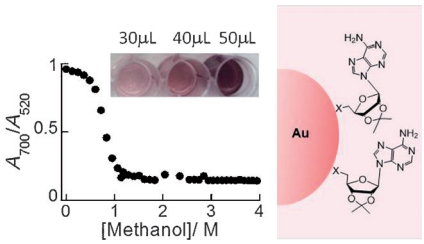

Nucleosides

J. P. Vanegas, L. E. Peisino, S. Pocoví-Martínez, R. J. Zaragozá, E. Zaballos-García, J. Pérez-Prieto** ..... ▮▮▮▮–▮▮▮▮

Unzipping Nucleoside Channels by Means of Alcohol Disassembly

